Near-infrared light-activated nanoprobe for simultaneous detection of hydrogen polysulfide and sulfur dioxide in myocardial ischemia-reperfusion injury

Xianzhu Luo[a], Cuiling Zhang[a*], Chenyang Yue[a], Yuelin Jiang[a], Fei Yang[a], Yuezhong Xian[a*]

[a] *Shanghai Engineering Research Center of Molecular Therapeutics and New Drug Development, Department of Chemistry, School of Chemistry and Molecular Engineering, East China Normal University, Shanghai 200241, China.*

**E-mail: clzhang@chem.ecnu.edu.cn; yzxian@chem.ecnu.edu.cn.*

Content:

1. Methods and procedures

Reagents and Instruments.

Naphthalene-1,8-dicarboxylic anhydride, 2,3,3-trimethyl-3H-indole, 3-bromopropanoic acid, methyl 2-(bromomethyl)-3-nitrobenzoate, tert-butyl (2-aminoethyl)carbamate, 5-nitrosalicylaldehyde, phenol, hydroiodic acid, potassium carbonate, 1-ethyl-3-(3-dimethylaminopropyl) carbodiimide hydrochloride and 1-hydroxybenzotriazole were purchased from Energy-chemical. RSL3, erastin, and ferrostatin-1 was obtained from Macklin. The hydropersulfides of cysteine and glutathione solution were synthesized according to previously reported literature and was used immediately.[1, 2] For GSSH synthesis, 2 mM glutathione (oxidized form) reacted with 2 mM freshly sodium sulfide (Na_2S) in 20 mM Tris-HCl buffer (pH 7.4) at 37 ºC for 15 min. CysSSH was synthesized as the the same way of synthesis of GSSH, instead of L-Cystine (oxidized form). Papain, CysSSCys and CH_3SSSCH_3 were purchased from Shanghai Titan Technology. GAPDH was obtained from Shanghai Yuanye Technology Co. All other chemical reagents were purchased from Sinopharm Chemical Reagent Co., Ltd. (Shanghai, China).

NMR experiments were performed on Bruker Advance II NMR spectrometer (Germany). The fluorescence and absorption spectra were collected on a Hitachi F-7000 spectrophotometer (Japan) and UV-2550 spectrophotometer (Japan), respectively. Cell images were obtained using a Nikon C2 confocal laser scanning microscope (Japan).

2. Response mechanism of light-activated probe.

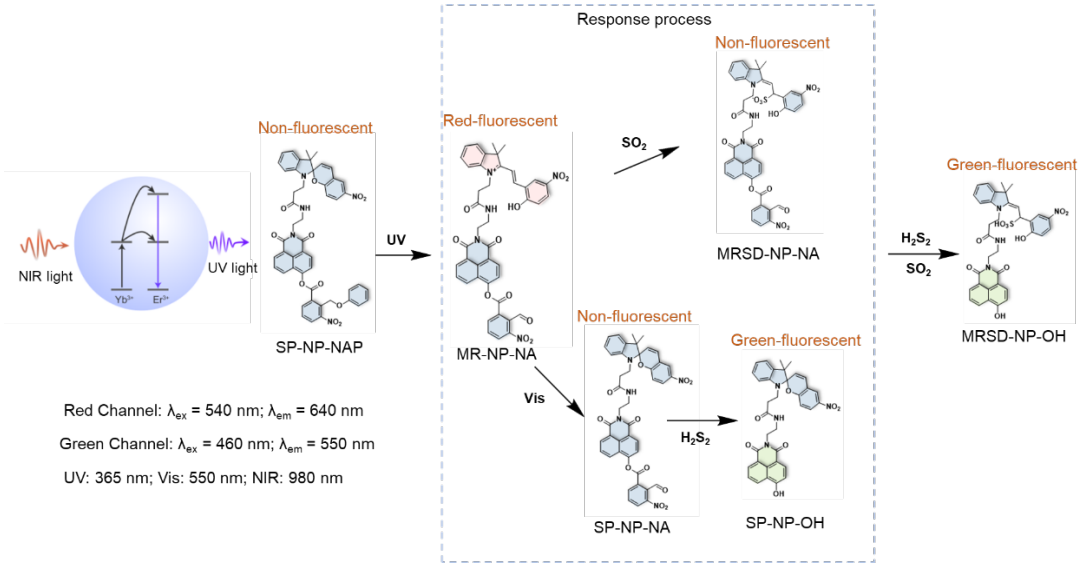

Scheme S1. Response mechanism of light-activated probe SP-NP-NAP to H_2S_n and SO_2.

3. Synthesis of probe SP-NP-NAP

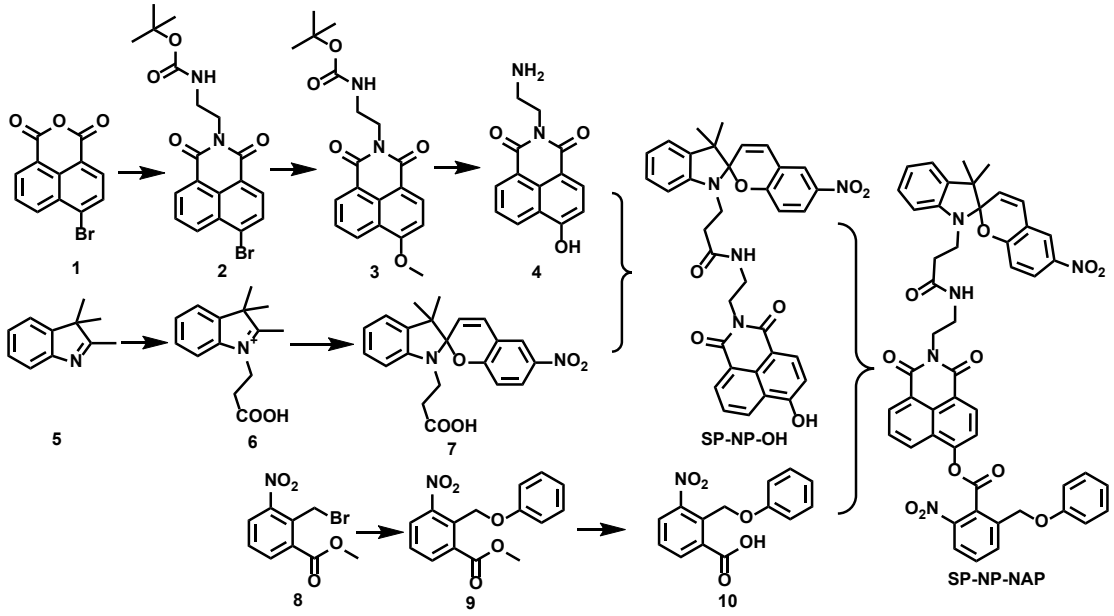

Fig. S1. The general synthesis routes for the probe SP-NP-NAP.

Synthesis of compound 2.

Compound 1 (2.77 g, 10 mmol) and tert-Butyl (2-aminoethyl)carbamate (1.6 mL, 20 mmol) were added to a round-bottomed flask containing 100 mL of absolute ethanol, and heated to reflux overnight. After the reaction is complete, suction filtration, dry, and directly use in the next step without treatment. ^{1}H NMR (500 MHz, $CDCl_3$) δ (ppm)

8.76 – 8.65 (m, 1H), 8.60 (d, J = 8.4 Hz, 1H), 8.45 (d, J = 7.9 Hz, 1H), 8.07 (d, J = 7.9 Hz, 1H), 7.93 – 7.81 (m, 1H), 4.94 (s, 1H), 4.38 (t, J = 5.6 Hz, 2H), 3.56 (d, J = 5.4 Hz, 2H), 1.29 (s, 9H).

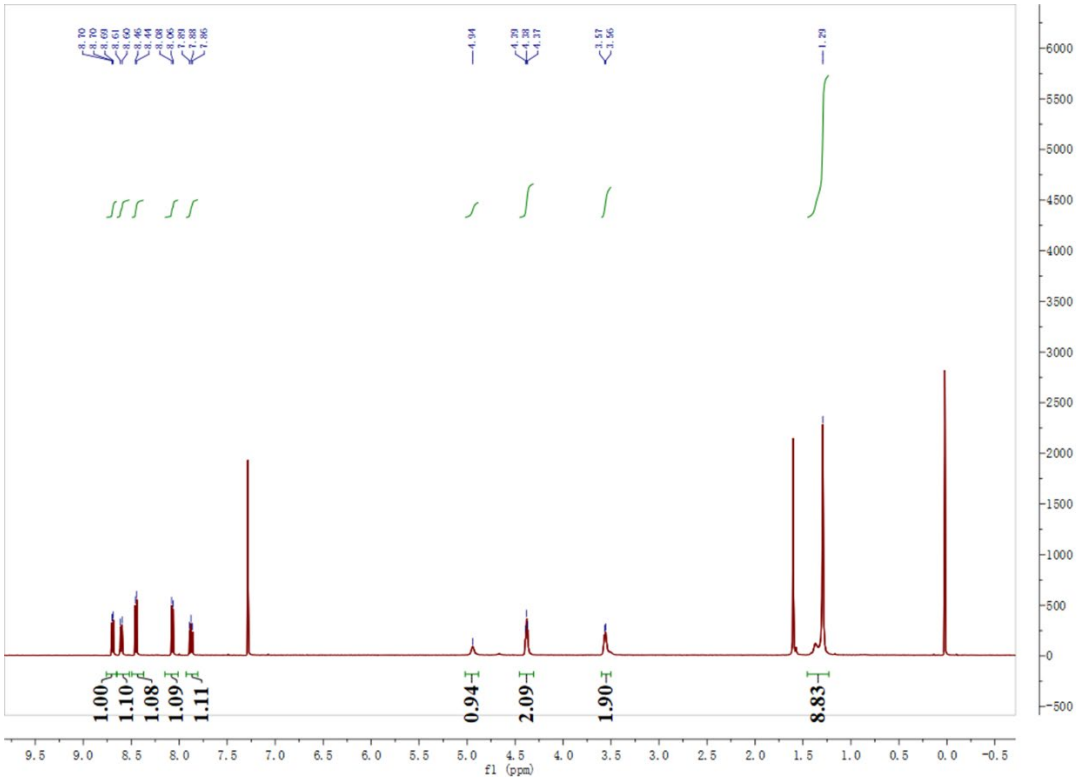

Fig. S2. ^{1}H NMR of compound 2.

Synthesis of compound 3.

Compound 2 (3.03 g, 6.3 mmol) and K_2CO_3 (7 g, 50 mmol) were added to a round-bottomed flask containing 100 mL of anhydrous methanol. The mixture was heated and refluxed for overnight. After the reaction was complete, the mixture was poured into water and yellow solids appeared. The crude product was purified it by silica gel chromatography (200-300 mesh) with a gradient eluent of CH_2Cl_2 and MeOH (100: 1-30: 1, v/v) to obtain compound 3 as a yellow solid. ^{1}H NMR (500 MHz, $CDCl_3$) δ 8.76 – 8.65 (m, 1H), 8.60 (d, J = 8.4 Hz, 1H), 8.45 (d, J = 7.9 Hz, 1H), 8.07 (d, J = 7.9 Hz, 1H), 7.93 – 7.81 (m, 1H), 4.94 (s, 1H), 4.38 (t, J = 5.6 Hz, 2H), 3.56 (d, J = 5.4 Hz, 2H), 1.29 (s, 9H).

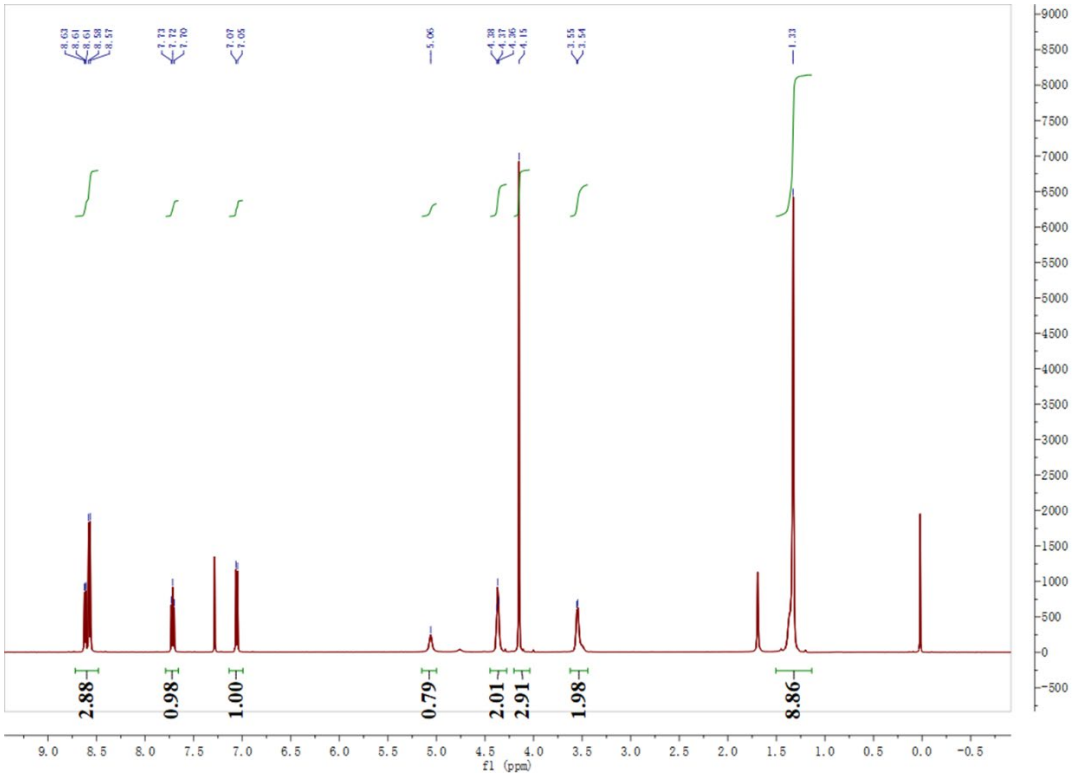

Fig. S3. ^{1}H NMR of compound 3.

Synthesis of compound 4.

Compound 3 (1.85 g, 5 mmol) and hydriodic acid (30 mL) were added to a 50 mL round-bottomed flask and heated to reflux at 140 °C overnight. After the reaction was completed, a large amount of yellow solid appeared, filtered and washed with a large amount of water. The yellow solid was vacuum-dried at 60 °C without any treatment and directly put into the next step. ^{1}H NMR (500 MHz, DMSO) δ (ppm) 11.97 (s, 1H), 8.57 (dd, J = 8.3, 1.2 Hz, 1H), 8.49 (dd, J = 7.3, 1.2 Hz, 1H), 8.38 (d, J = 8.2 Hz, 1H), 7.80 (dd, J = 8.3, 7.3 Hz, 3H), 7.19 (d, J = 8.2 Hz, 1H), 4.29 (t, J = 5.8 Hz, 2H), 3.14 (dd, J = 11.3, 5.7 Hz, 2H).

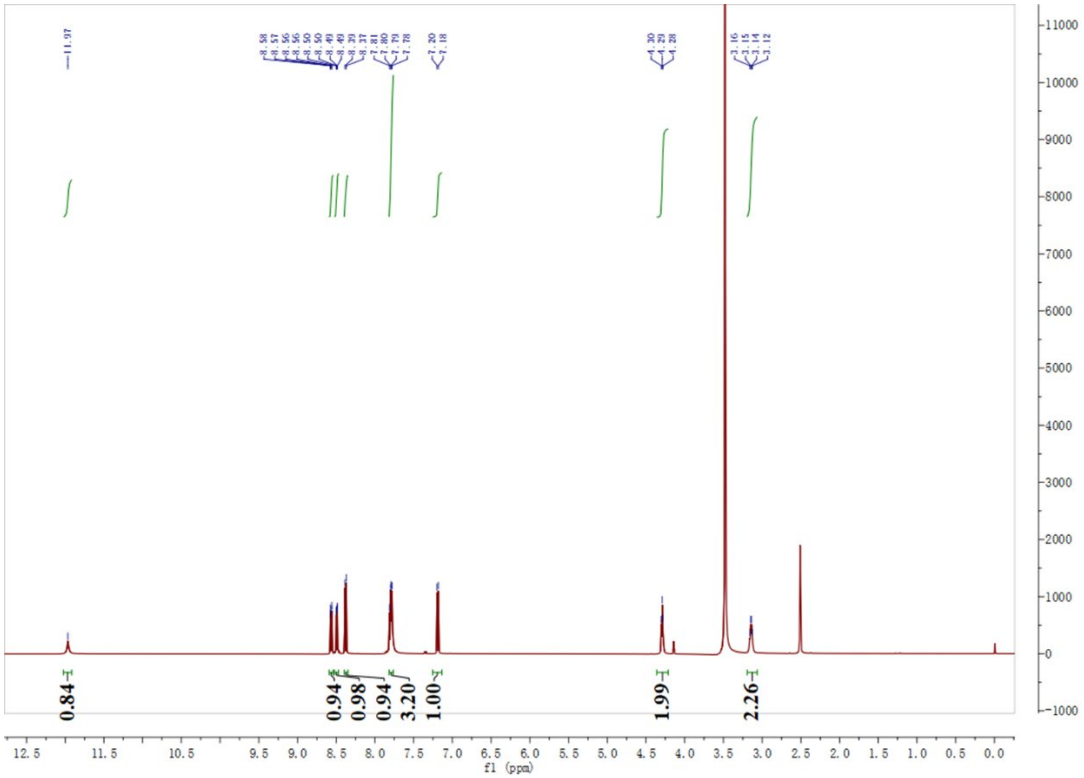

Fig. S4. ^{1}H NMR of compound 4.

Synthesis of compound 6.

A mixture of 2,3,3-trimethyl-3H-indole (1.59 g, 10 mmol) and 3-bromo-propionic acid (1.51 g, 10 mmol) was dissolved in dry CH_3CN (50 mL), and the mixture was refluxed for 12 h. After the reaction was completed, the solvent was removed to obtain a dark purple residue. The crude product was quickly passed through column chromatography with a gradient eluent of CH_2Cl_2. The solution was concentrated, and added dropwise to anhydrous ether, a large amount of pink solid appeared. The solids were collected and dried in vacuo. ^{1}H NMR (500 MHz, DMSO) δ (ppm) 8.00 (dd, J = 6.0, 2.9 Hz, 1H), 7.87 – 7.77 (m, 1H), 7.62 (dd, J = 5.5, 3.3 Hz, 2H), 4.65 (t, J = 7.0 Hz, 2H), 2.98 (t, J = 7.0 Hz, 2H), 2.86 (s, 3H), 1.53 (s, 6H).

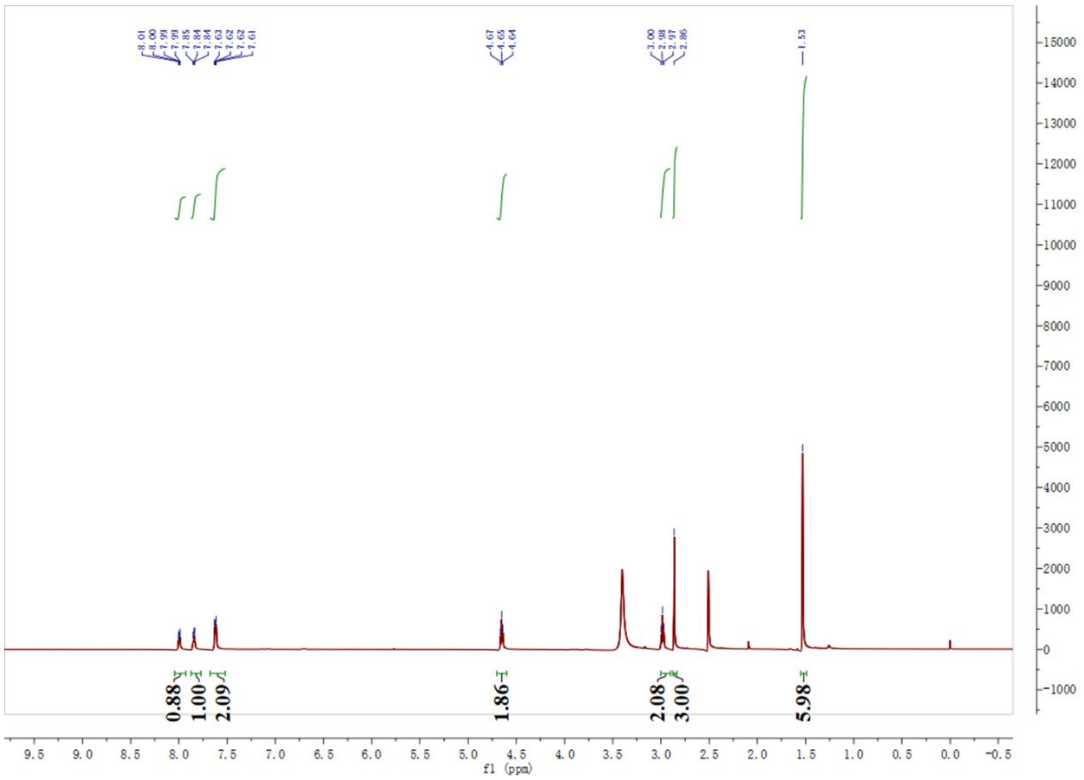

Fig. S5. ^{1}H NMR of compound 6.

Synthesis of compound 7.

Compound 6 (2.32 g, 10 mmol), 5-nitrosalicylaldehyde (1.83 g, 11 mmol) and triethylamine (1.7 mL, 12 mmol) in dry EtOH (50 mL) were refluxed for overnight in the dark. After completion of the reaction, the mixture was cooled to room temperature, the resulting precipitate was filtered and washed with cold EtOH to give a brown powder. ^{1}H NMR (500 MHz, DMSO) δ (ppm) 12.23 (s, 1H), 8.22 (d, J = 2.7 Hz, 1H), 8.01 (dd, J = 9.0, 2.7 Hz, 1H), 7.22 (d, J = 10.4 Hz, 1H), 7.13 (d, J = 6.4 Hz, 2H), 6.87 (d, J = 9.0 Hz, 1H), 6.81 (t, J = 7.4 Hz, 1H), 6.67 (d, J = 8.0 Hz, 1H), 6.00 (d, J = 10.4 Hz, 1H), 3.54 – 3.38 (m, 2H), 2.57 (dd, J = 15.5, 7.7 Hz, 1H), 2.47 – 2.42 (m, 1H), 1.19 (s, 3H), 1.08 (s, 3H).

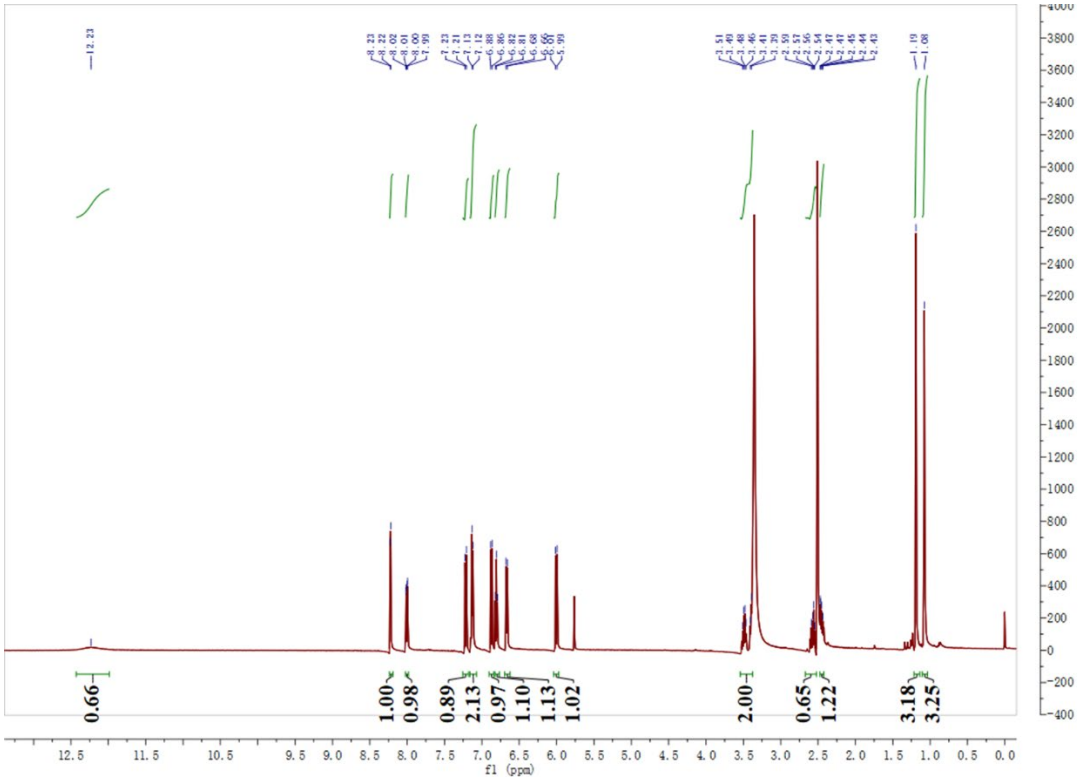

Fig. S6. ^{1}H NMR of compound 7.

Synthesis of compound 9.

Compound 8 (0.54 g, 2 mmol), phenol (0.3 g, 3 mmol) and potassium carbonate (0.83 g, 6 mmol) in dry acetonitrile (50 mL) were heated to reflux overnight. After the reaction was completed, the solvent was removed. The crude product was purified by silica gel chromatography (200-300 mesh) with a gradient eluent of petroleum ether and CH_2Cl_2 (8: 1-5: 1, v/v) to obtain compound 9 as a beige oily liquid. ^{1}H NMR (500 MHz, $CDCl_3$) δ (ppm) 8.01 (dd, J = 7.8, 1.3 Hz, 1H), 7.95 (dd, J = 8.1, 1.3 Hz, 1H), 7.57 (t, J = 7.9 Hz, 1H), 7.34 – 7.28 (m, 2H), 7.01 (dd, J = 10.6, 4.1 Hz, 1H), 6.93 (dd, J = 8.7, 0.9 Hz, 2H), 5.56 (s, 2H), 3.87 (s, 3H).

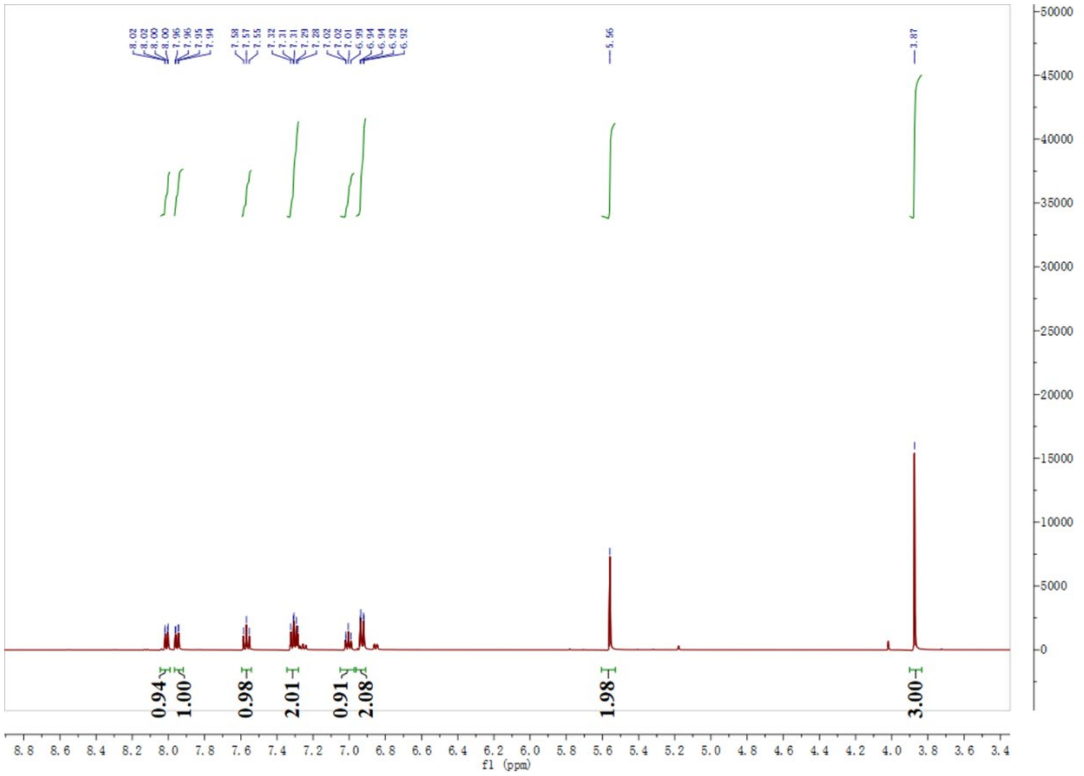

Fig. S7. ^{1}H NMR of compound 9.

Synthesis of compound 10.

A solution of compound 2 (1.1 g, 4 mmol) and sodium hydroxide (0.32 g, 8 mmol) in ethanol-water (8:2, 10 mL) was refluxed for 6 h. The solvent was evaporated and dissolving the residue in water. The solution was neutralized with hydrochloric acid and extracted by ethyl acetate. Then organic layer was washed with brine, dehydrated with anhydrous Na_2SO_4, and concentrated under reduced pressure. The crude material was purified by flash column chromatography to give compound 10 as white solid. ^{1}H NMR (500 MHz, DMSO) δ (ppm) 7.75 (d, J = 7.7 Hz, 1H), 7.62 (d, J = 7.9 Hz, 1H), 7.43 (t, J = 7.8 Hz, 1H), 7.26 – 7.22 (m, 2H), 6.92 – 6.89 (m, 3H), 5.64 (s, 2H).

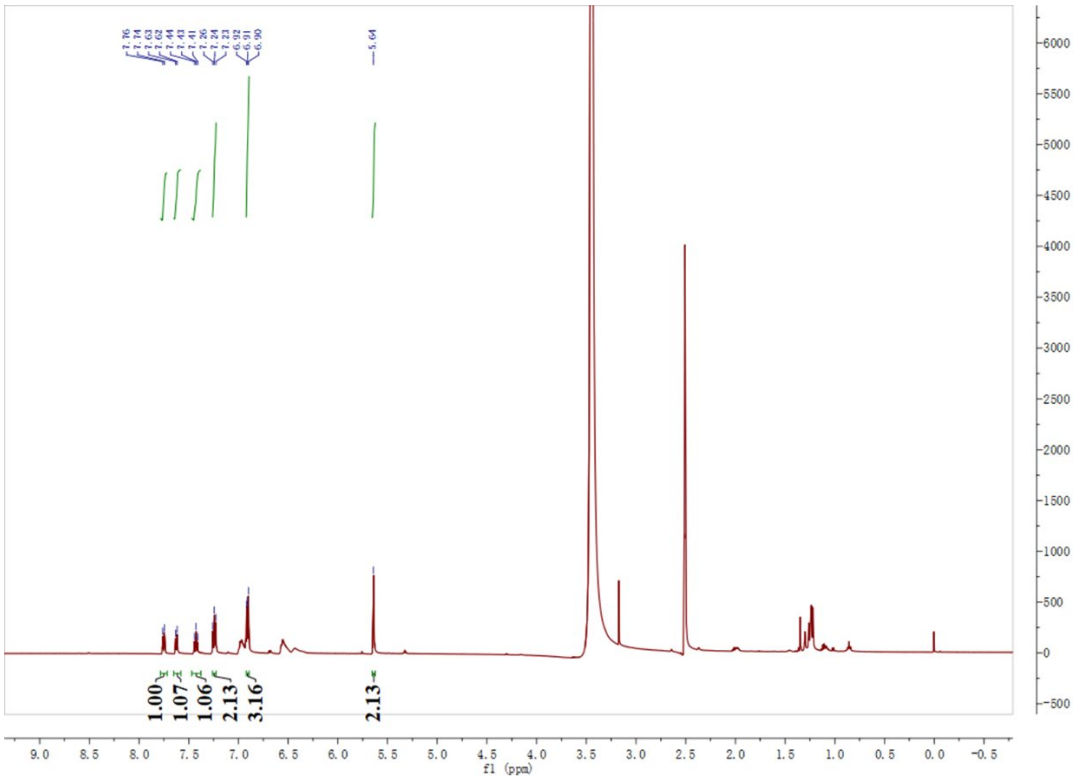

Fig. S8. ^{1}H NMR of compound 10.

Synthesis of compound SP-NP-OH.

The solution of compound 7 (0.38 g, 1 mmol), 1-Ethyl-3-(3-dimethylaminopropyl) carbodiimide hydrochloride (EDCl, 0.38 g, 2 mmol) and 1-Hydroxybenzotriazole (HOBt, 0.27 g, 2 mmol) was stirred in dried DMF at 0 °C under N_2 for 30 min. Then, compound 4 (0.13 g, 0.5 mmol) and triethylamine (0.15 mL) were sequentially added. The resulting mixture was stirred at room temperature for 24 h, and then poured into water and filtered to yield a gray powder. This powder was purified by column chromatography on silica gel chromatography (200-300 mesh) (CH_2Cl_2: MeOH= 30:1 v/v) to afford SP-NP-OH. ^{1}H NMR (500 MHz, DMSO) δ (ppm) 11.86 (s, 1H), 8.54 (d, J = 8.4 Hz, 1H), 8.44 (d, J = 6.4 Hz, 1H), 8.33 (d, J = 8.2 Hz, 1H), 8.21 (d, J = 2.8 Hz, 1H), 8.10 – 7.95 (m, 2H), 7.82 – 7.70 (m, 1H), 7.17 (dd, J = 11.0, 9.4 Hz, 2H), 7.12 – 7.03 (m, 2H), 6.85 (d, J = 9.0 Hz, 1H), 6.78 (t, J = 7.4 Hz, 1H), 6.59 (d, J = 7.7 Hz, 1H), 5.95 (d, J = 10.4 Hz, 1H), 4.09 (t, J = 6.0 Hz, 2H), 3.32 – 3.26 (m, 2H), 2.24 (ddd, J = 14.1, 12.8, 6.8 Hz, 2H), 1.27 – 1.21 (m, 2H), 1.17 (s, 3H), 1.06 (s, 3H). ^{13}C NMR (126 MHz, DMSO) δ (ppm) 170.9, 164.5, 163.7, 160.6, 159.6, 140.9, 133.9, 131.5, 129.2,

128.5, 128.0, 126.1, 123.2, 122.9, 122.5, 122.3, 122.1, 119.5, 119.3, 115.9, 113.3, 110.3, 106.9, 52.9, 37.0, 35.2, 26.1, 19.9. HPLC-HRMS: m/z [$C_{35}H_{30}N_4O_7$], calcd, 618.2114; found $[M+Na]^+$: 641.2012.

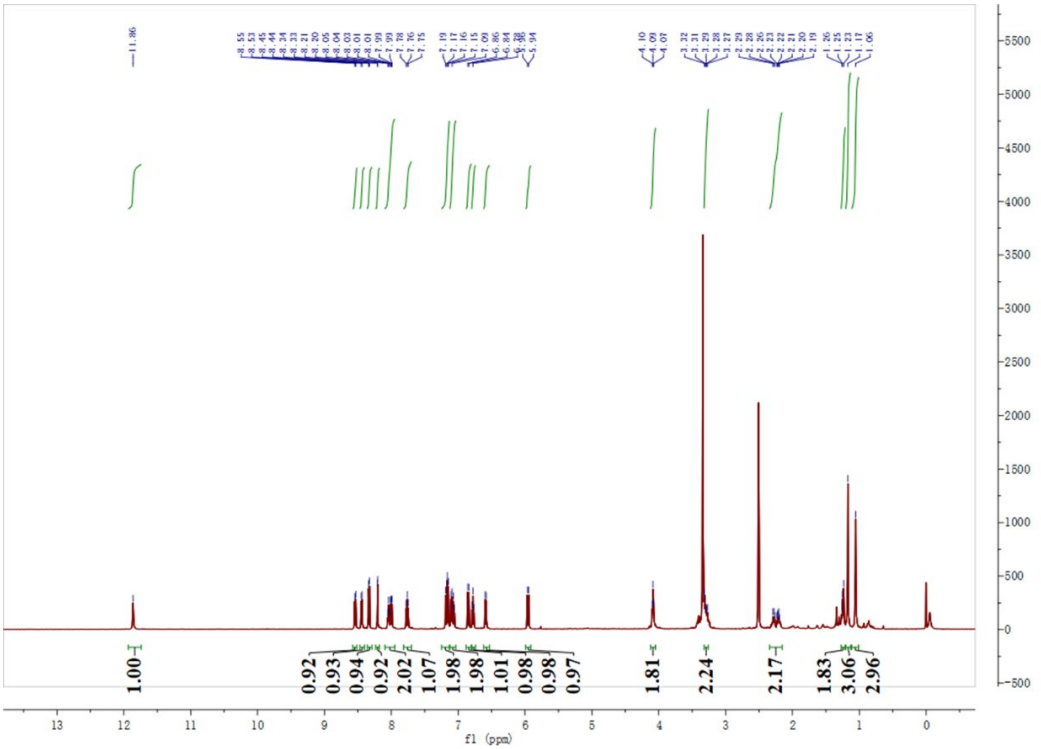

Fig. S9. ^{1}H NMR of compound SP-NP-OH.

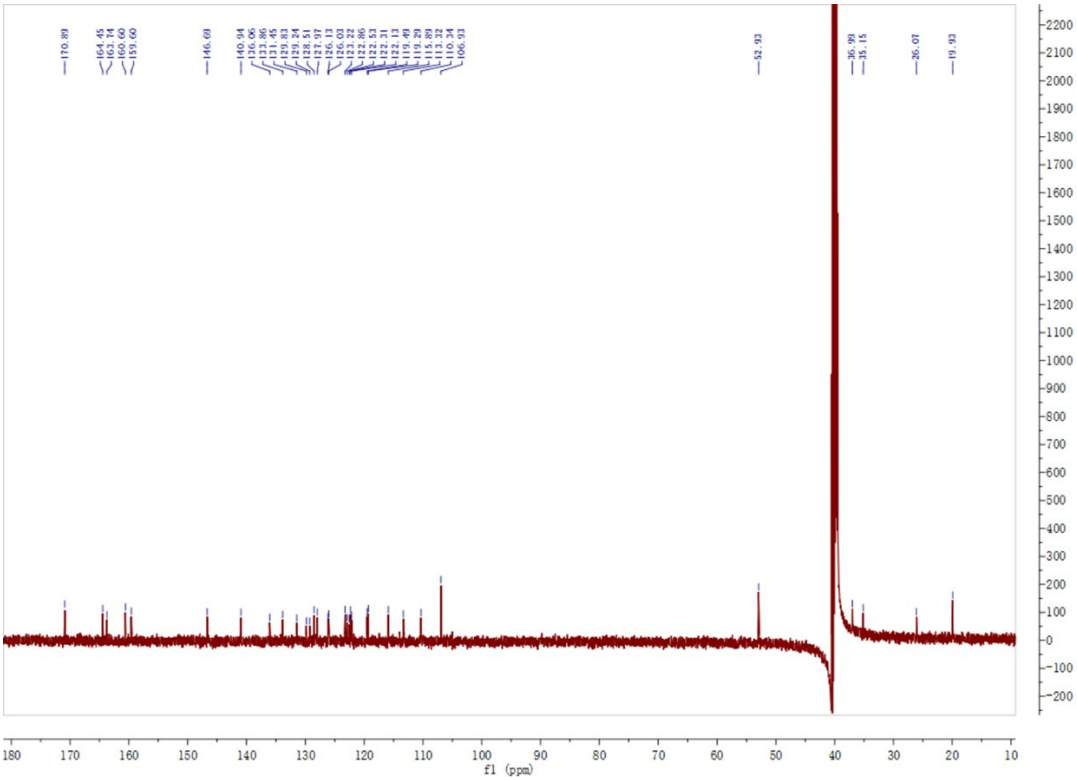

Fig. S10. ^{13}C NMR of compound SP-NP-OH.

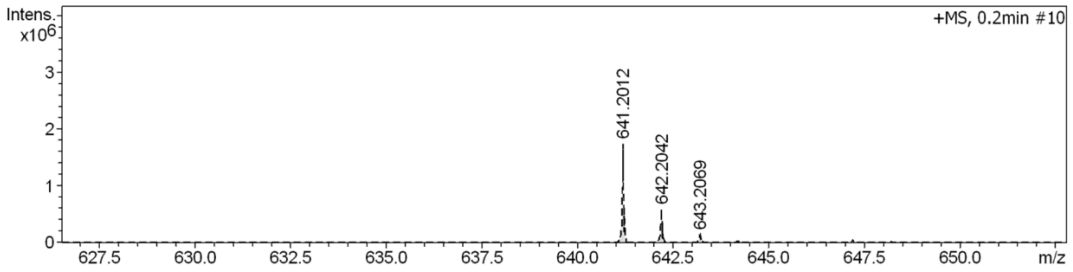

#	m/z	Res.	S/N	I	I %	FWHM
1	641.2012	24539	1517.8	1728484	100.0	0.0261
2	642.2042	20267	512.2	581384	33.6	0.0317
3	643.2069	14316	113.6	128764	7.4	0.0449

Meas. m/z	#	Ion Formula	m/z	err [ppm]	mSigma		Score	rdb	e¯ Conf	N-Rule
641.2012	1	C35H30N4NaO7	641.2007	-0.8	32.7	4	100.00	22.5	even	ok

Fig. S11. HR-MS of compound SP-NP-OH.

Synthesis of compound SP-NP-NAP. Compound 10 (0.1 g, 0.375 mmol) was dissolved in 10 mL of anhydrous dichloromethane under an ice bath, about 1 mL of thionyl chloride was added, and then the reaction was carried out at room temperature for about 2 h. The excess thionyl chloride was removed to obtain the corresponding acid chloride compound. Compounds SP-NP-OH (0.155 g, 0.25 mmol) and Et_3N (0.08 mL, 0.5 mmol) were dissolved in dry chloroform under an ice bath and stirred for about 30 min. The prepared acid chloride was slowly added dropwise to the mixture and stirred at room temperature for about 4 h. Rotary evaporation to remove the solvent. Crude product was purified by column chromatography on silica (CH_2Cl_2: MeOH = 50:1 v/v) to afford probe SP-NP-NAP. ^{1}H NMR (500 MHz, $CDCl_3$) δ (ppm) 8.61 – 8.50 (m, 2H), 8.41 (dd, *J* = 7.7, 1.0 Hz, 1H), 8.35 – 8.28 (m, 1H), 8.15 (dd, *J* = 8.2, 1.1 Hz, 1H), 8.00 – 7.92 (m, 2H), 7.78 (t, *J* = 8.0 Hz, 1H), 7.71 (dd, *J* = 8.3, 7.4 Hz, 1H), 7.63 (d, *J* = 8.1 Hz, 1H), 7.30 (s, 1H), 7.26 (t, *J* = 2.0 Hz, 1H), 7.14 – 7.09 (m, 1H), 7.01 (t, *J* = 7.4 Hz, 1H), 6.96 – 6.89 (m, 3H), 6.87 (d, *J* = 10.4 Hz, 1H), 6.79 – 6.70 (m, 2H), 6.59 (d, *J* = 7.8 Hz, 1H), 6.16 (s, 1H), 5.80 (d, *J* = 10.4 Hz, 1H), 5.69 (s, 2H), 4.35 (t, *J* = 5.4 Hz, 2H), 3.66 – 3.57 (m, 2H), 2.50 (dd, *J* = 14.7, 7.4 Hz, 1H), 2.37 – 2.28 (m, 1H), 1.29 (d, *J* = 16.0 Hz, 2H), 1.20 (s, 3H), 1.02 (s, 3H). ^{13}C NMR (126 MHz, $CDCl_3$) δ (ppm) 171.4, 164.5, 164.0, 159.4, 157.9, 151.5, 151.2, 146.2, 141.0, 135.8, 134.0, 132.9, 132.0, 129.7, 129.5, 128.29, 127.8, 127.7, 127.6, 125.8, 125.1, 122.7, 122.2,

121.9, 121.6, 120.4, 119.5, 118.6, 115.4, 114.8, 106.7, 63.3, 52.9, 39.8, 39.7, 39.4, 35.6, 25.7, 19.7. HPLC-HRMS: m/z [$C_{49}H_{39}N_5O_{11}$], calcd, 873.2646; found $[M+Na]^+$: 896.2554.

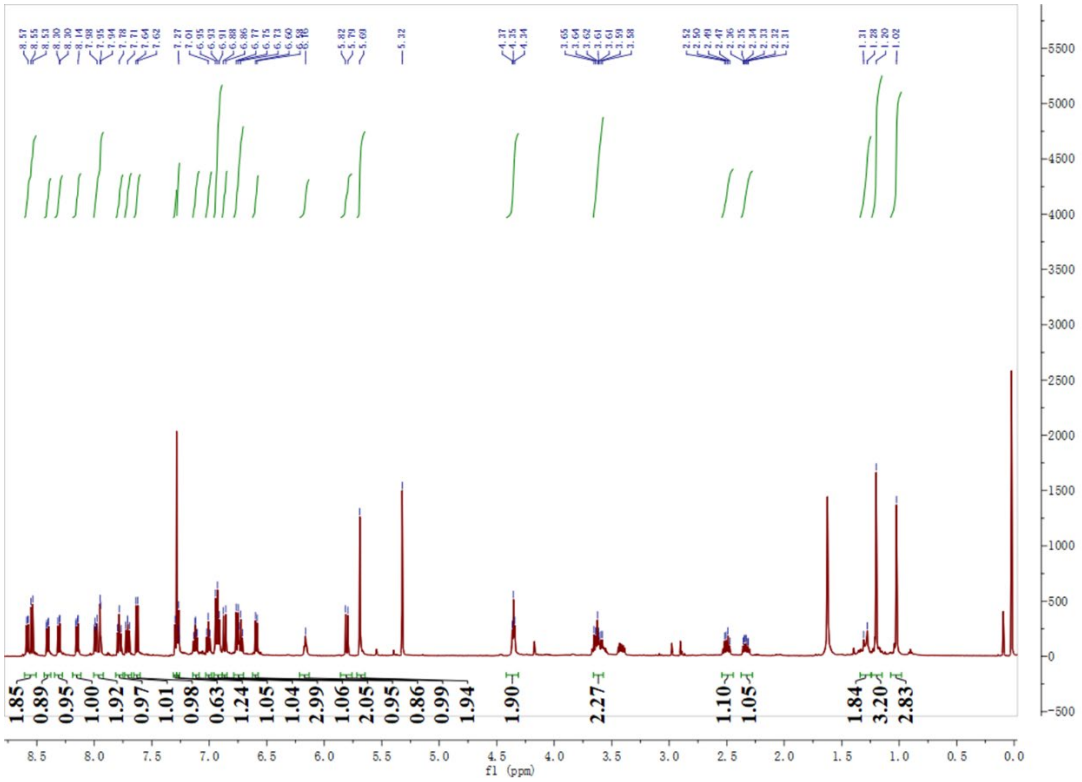

Fig. S12. ^{1}H NMR of compound SP-NP-NAP.

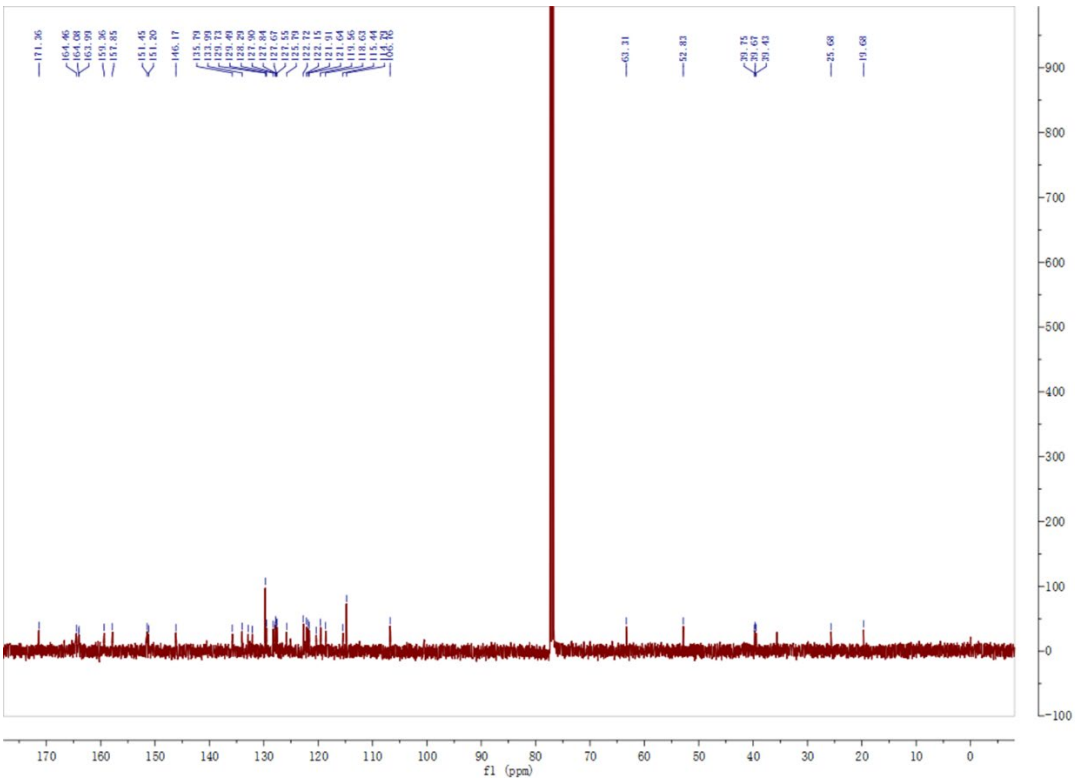

Fig. S13. ^{13}C NMR of compound SP-NP-NAP.

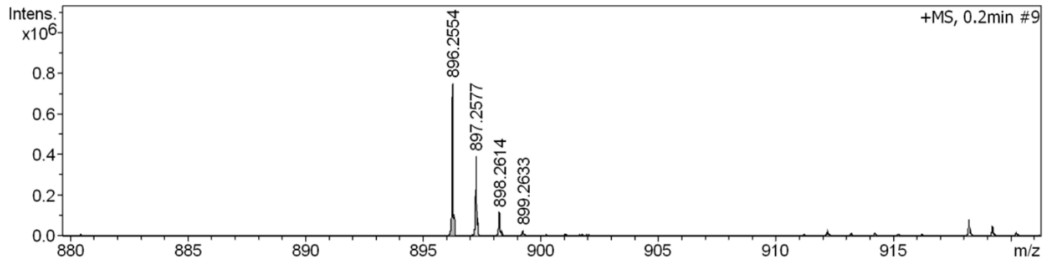

#	m/z	Res.	S/N	I	I %	FWHM
1	896.2554	29189	1015.2	750772	100.0	0.0307
2	897.2577	23518	528.1	390300	52.0	0.0382
3	898.2614	19859	158.8	117264	15.6	0.0452
4	899.2633	19035	37.8	27880	3.7	0.0472

Meas. m/z	#	Ion Formula	m/z	err [ppm]	mSigma		Score	rdb	e¯ Conf	N-Rule
896.2554	1	C49H39N5NaO11	896.2538	-1.7	18.6	1	60.54	32.5	even	ok

Fig. S14. HR-MS of compound SP-NP-NAP.

4. Synthesis of the UCNP@mSiO$_2$@SP-NP-NAP nanoparticles.

4.1 Synthesis of Core of NaYF$_4$: Yb/Tm UCNPs.

The synthesis of monodisperses core-shell structured UCNPs (CS UCNPs, NaYF$_4$:30%Yb, 0.5%Tm@NaYF$_4$) were carried out. Firstly, the core structure of UCNPs (NaYF$_4$: Yb/Tm) was synthesized. The aqueous solution containing YbCl$_3$·6H$_2$O (0.6 mmol), YCl$_3$·6H$_2$O (1.39 mmol), and TmCl$_3$·6H$_2$O (0.01 mmol) was added into 30 mL of 1-octadecene and 15 mL of oleic acid. The solution was heated to 156 °C for 1 h to remove the water under Ar$_2$. Cooling to room temperature (25 °C), the methanol solution of NH$_4$F (8 mmol) and NaOH (5 mmol) was added to the mixture. After stirring for 2 h, the solution was heated to about 100 °C to remove methanol. Then it was rapidly heated to 300 °C for around 1 h. Cooling to room temperature (25 °C) with the flow of Ar$_2$, the product was precipitated by adding ethanol. NaYF$_4$: Yb/Tm UCNPs were obtained by centrifugation and washed three times with cyclohexane and ethanol, and finally redispersed in 20 mL of cyclohexane.

4.2 Synthesis of Core-Shell Structure of NaYF$_4$: Yb/Tm@NaYF$_4$.

The aqueous solution containing YCl$_3$·6H$_2$O was added to 30 mL 1-octadecene and 15 mL oleic acid. Subsequently, the mixture was heated to 156 °C for 1 h. After cooling to room temperature (25 °C), the core UCNPs (NaYF$_4$: Yb/Tm) were added into mixture and then the solution was heated for removing cyclohexane. Next, the solution

NH_4F and NaOH in methanol was added to the mixture. Then, the methanol was removed, and the temperature was fast heated to 300 °C and maintained for 1 h. The product $NaYF_4$: Yb/Tm@$NaYF_4$ nanocrystal was obtained by the same postprocessing steps as those for $NaYF_4$: Yb/Tm UCNPs.

4.3 Synthesis of the UCNP@$mSiO_2$ nanoparticles.

The hexadecyltrimethylammonium bromide (CATB, 0.2 g) ino 20 mL water was mixed with UCNP in cyclohexane. After stirred for about 1 h, the transparent solution was obtained. Then, the solution was heated to 70 °C and maintained for about 30 min. After cooled to room temperature, 20 mL of water, 3 mL of ethanol, and 0.2 M NaOH was added to adjust the pH to 10-11. Heated to 70 °C, TEOS (100 μL) was added dropwise and stirred for about 0.5 h. Cooled to room temperature, centrifuged, the solid was collected and washed with ethanol for three time. Subsequently, a methanolic solution (20 mL) of 1 wt% NaCl was refluxed overnight and the solid was collected by centrifugation to give UCNP@$mSiO_2$.

4.4 Synthesis of the UCNP@$mSiO_2$@SP-NP-NAP nanoparticles.

The compound SP-NP-NAP was dissolved in 2 mL of dichloromethane and was add dropwise to UCNP@$mSiO_2$ dispersed in ethanol solution with vigorous stirring for about 36 h under dark condition. Centrifuge, remove the solution and wash with dichloromethane and ethanol to obtain a dark red solid, UCNP@$mSiO_2$@SP-NP-NAP.

5. Cell culture and model establishment

5.1 Cell culture and confocal imaging.

The human cervical cancer cells (HeLa cells) and the rat cardiac cells (H9C2 cells) were obtained from the Committee on Type Culture Collection of Chinese Academy of Sciences (Shanghai, China). HeLa cells and H9C2 cells were incubated in DMEM supplemented with 10% FBS and 1% antibiotics (penicillin/streptomycin, 100 μg/mL) at 37 °C in a 5% CO_2 atmosphere. All groups were treated with nanoprobe (200 μg/mL) for 2.5 h. After nanoprobe entered cells, the extracellular nanoprobes were washed with PBS at least 4 times. In order to image the intracellular H_2S_2 and SO_2, the nanoprobes in cells were activated by NIR (980 nm) for 30 min, and the fluorescence was recorded

excited by 561 nm and 488 nm laser light, respectively. Subsequently, these cells were exposed under visible light (550 nm) for 10 min, and then, the fluorescence was recorded excited by 561 nm and 488 nm laser light, respectively. Vis irradiation is performed after NIR irradiation. Therefore, the monitoring of SO_2 was mainly based on the changes of fluorescent signal in the red channel after NIR light activation, while the detection of H_2S_n was mainly resulted from the changes in the green channel through NIR and Vis light activation.

5.2 Cell viability assay.

The cytotoxicity of probe was evaluated by CCK-8 assay. The tested cells (5.0×10^3 cells/well) were put in a 96-well plate and then incubated for 24 h. Subsequently, a series of concentrations of nanoprobe (0-400 μg/mL) were added into the wells. After the cells were incubated for 24 h at 37 °C under 5% CO_2, 10 μL CCK-8 solution was added to each well of the plate and incubated for 4 h at 37 °C under 5% CO_2. Then, the optical density (OD) was measured at 450 nm using a microplate reader (Tecan, Austria). The following formula was used to calculate the viability of cell growth: Viability (%) = (mean of absorbance value of treatment group - blank)/(mean absorbance value of control - blank) × 100.

5.3 Establishment of cellular models.

For the detection of exogenous SO_2 and H_2S_2, HeLa cells were treated with different concentrations of Na_2SO_3 (50 μM), H_2S_2 (50 μM), and Na_2SO_3 (50 μM)+H_2S_2 (50 μM), respectively. Subsequently, cells were imaged after 3 h of incubation with UCNP@mSiO_2@SP-NP-NAP. The detection of endogenous SO_2 and H_2S_2 was performed for different groups, including control group (without any treatments), GSH + $Na_2S_2O_3$ group (cells pretreated with 200 μM $Na_2S_2O_3$ and 500 μM GSH for 60 min), Cys group (cells pretreated with 200 μM Cys for 60 min), and LPS group (cells pretreated with 1 μg/mL LPS for 12 h). Then, the cells were imaged after 3 h of incubation with UCNP@mSiO_2@SP-NP-NAP.

In order to establish ferroptosis model in cardiac machine cells, H9C2 cells were treated with different ferroptosis inducers (RSL3 or erastin) and then co-incubated with

the UCNP@mSiO$_2$@SP-NP-NAP for 3 h before confocal imaging. The variation of SO_2 and H_2S_2 levels in different groups was measured, including control group (H9C2 cells cultured with UCNP@mSiO$_2$@SP-NP-NAP), RSL3 group (H9C2 cells pretreated with 3.0 μM RSL3 for 6 h), RSL3 + Fer-1 group (cells co-incubated with 3.0 μM RSL3 () and 10.0 μM Fer-1for 6 h), Erastin group (cells pretreated with 10.0 μM erastinfor 2 h), and Erastin + Fer-1 group (cells co-incubated with 10.0 μM erastin and 10.0 μM Fer-1 for 2 h).

Establishment of I/R injury model in H9C2 cell.

The establishment of I/R injury model was based on literatures.[3, 4] To simulate myocardial I/R in vitro, H9C2 cells were cultured in confocal dishes until they adhered. Then, H9C2 cells were washed three times with PBS and then cultured in glucose-free DMEM medium. After that, the dishes were sealed within an airtight AnaeroPouch bag, which provided a near anaerobic conditions with O_2 concentration less than 1% (monitored with the oxygen indicator) and a CO_2 concentration of approximately 5%. The H9C2 cells were exposed to these conditions for 2.5 h. And then, the cells were incubated with high-glucose DMEM in a 5 % CO_2 and 95% O_2 atmosphere for 5 h.

Quantification Na_2SO_3 and H_2S_2 in cells.

A calibration curve was constructed by modification the referenences.[5-8] Different concentrations of Na_2SO_3 and H_2S_2 in the presence of UCNP@SP-NP-NAP were placed on confocal dishes containing cells and then imaged. Corresponding curves were obtained by the mean fluorescence intensity versus different concentrations of Na_2SO_3 and H_2S_2, respectively. The monitoring of SO_2 relied on the changes of signal in the red channel after NIR light activation, while the detection of H_2S_2 depended on the changes of signal in the green channel through NIR and Vis light activation.

Flow Cytometry Experiments.

Cells were treated as described in Cell Culture and Imaging. Before measurement by flow cytometry, cells were scraped off gently and collected into a clean 2 mL centrifuge tube. Then, cells were spun down (500 rpm, room temperature, 3 min). After discarding the supernatant, 1 mL of warm PBS was added gently to resuspend the cell

pellet. The detection of fluorescence signal via flow cytometry channel was chosen as FITC and Cy 5.5 channel.

Establishment of mouse I/R models.

All experimental procedures on mice were performed in compliance with the relevant laws and the Guidelines of Animal Experimental Ethics Committee of East China Normal University. All mice experiments have been approved by the committee (No. m20210224). Healthy mice were divided into three groups, including control group (100 μL saline 30 min before surgery), I/R group (100 μL saline 30 min before being subjected to ischemia), and I/R + Fer-1 group (1 mg/kg body weigh 30 min before being subjected to ischemia). For induction of myocardial I/R injury, the left intercostal thoracotomy and left anterior descending coronary artery (LAD) ligation were performed. Briefly, mice were initially anesthetized with isoflurane inhalation, a left open thoracotomy was performed in the third and fourth intercostal space rows of the mice to fully expose the left ventricle and left auricle. The left anterior descending branch (LAD) was ligated using a 7-0 wire. After 30 min of ischemia induction, the myocardium in the ischemic area was observed to turn white. The colour of the myocardium in the ischemic region was restored when the ligated wire was released and the mice were reperfused for 24 h. The ischemic region was then exposed to a 6-0 wire. At this time, different drugs were injected into the myocardium of the mice, and finally the muscles, ribs, and skin were sutured sequentially with a 5-0 wire. Mice in the control group underwent the same surgery but without ligation of the LAD. The tracheal tube was removed when the mice recovered from stable respiration, and the mice were placed on a heating blanket until they woke up spontaneously.

Statistical Analysis

Data were expressed as the means ± standard deviation (SD) of three parallel measurements. The significance of the difference was evaluated via a one-way analysis of variance. Statistical significance was set at *$P < 0.05$, **$P < 0.01$, ***$P < 0.001$, ****$P < 0.0001$.

6. Properties and spectral studies of SP-NP-NAP.

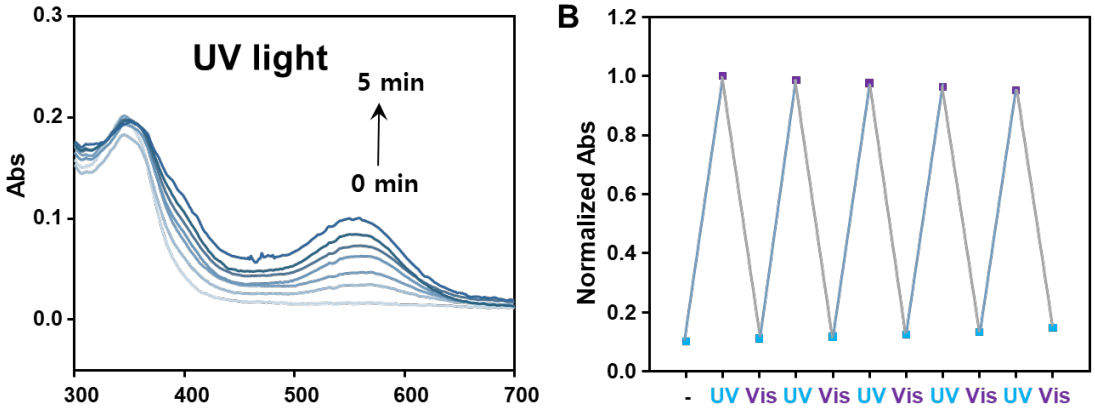

Fig. S15. (A) The absorption spectra of SP-NP-NAP activation with UV light (365 nm). (B) The photo-controlled switching behaviors of SP-NP-NAP based on the variation of absorbance signal at 560 nm under UV/Vis light irradiation.

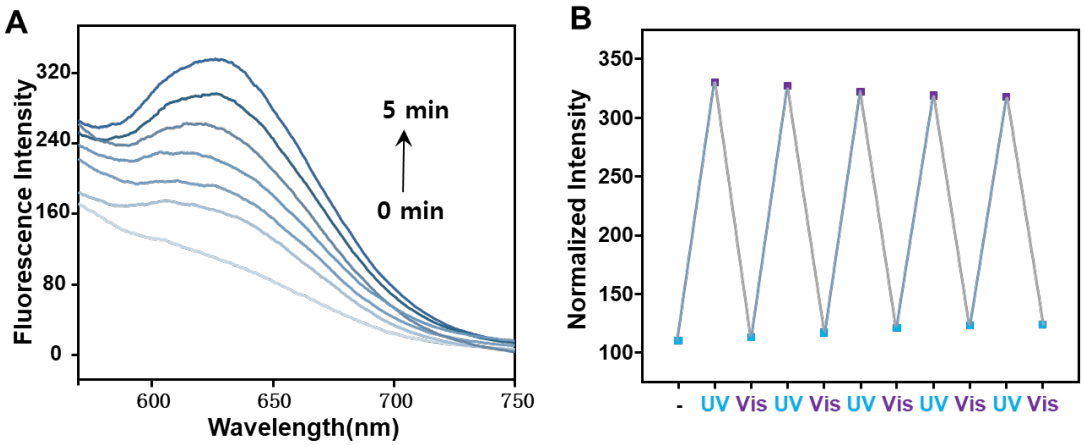

Fig. S16. (A) The fluorescence spectra of SP-NP-NAP activated with UV light and then excited by 540 laser light. (B) The photo-switching behaviors of SP-NP-NAP based on the variation of fluorescence signal at 640 nm under UV/Vis light activation.

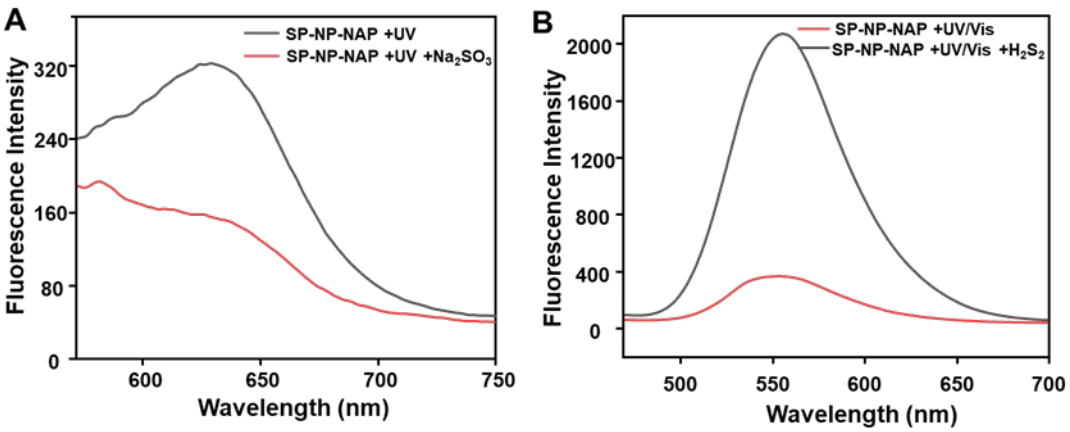

Fig. S17. The fluorescence spectra of SP-NP-NAP for detection of (A) Na_2SO_3 after UV light activation and then excited by 540 nm light, and (B) H_2S_2 through sequential UV/Vis light activation and then excited by 460 nm light.

7. Properties and spectral studies of UCNPs, UCNP@mSiO₂.

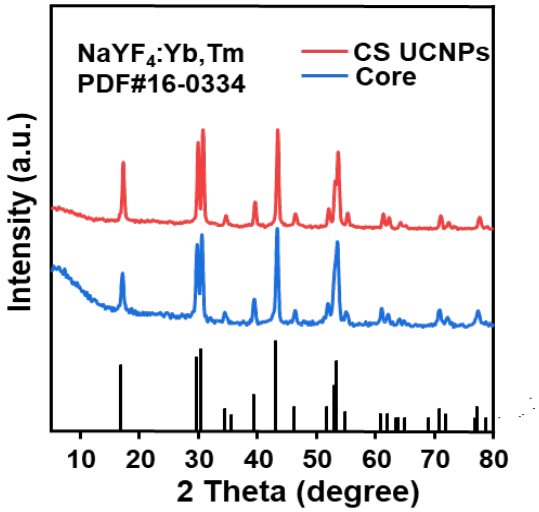

Fig. S18. XRD patterns of core ($NaYF_4$: Yb/Tm) and CS UCNPs ($NaYF_4$: Yb/Tm@$NaYF_4$).

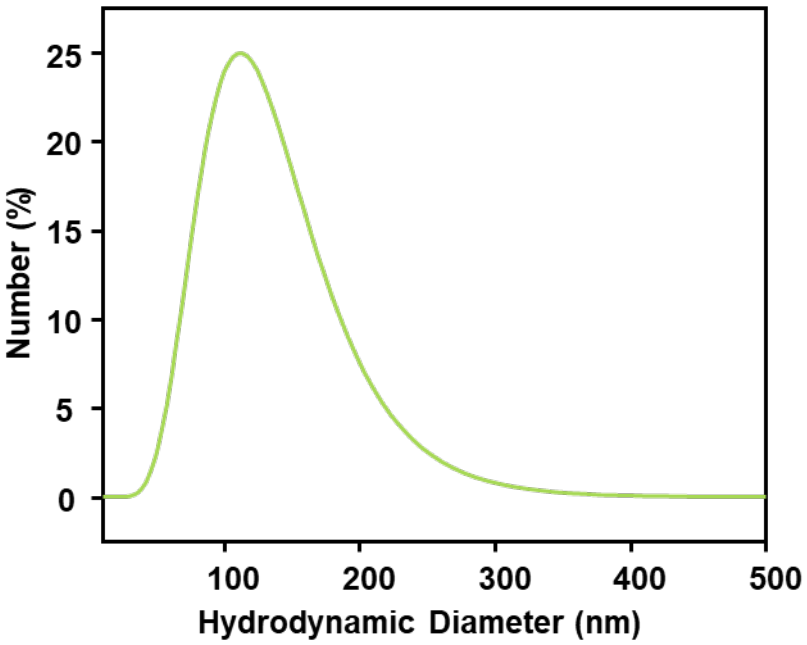

Fig. S19. The size distributions of UCNP@mSiO$_2$@SP-NP-NAP.

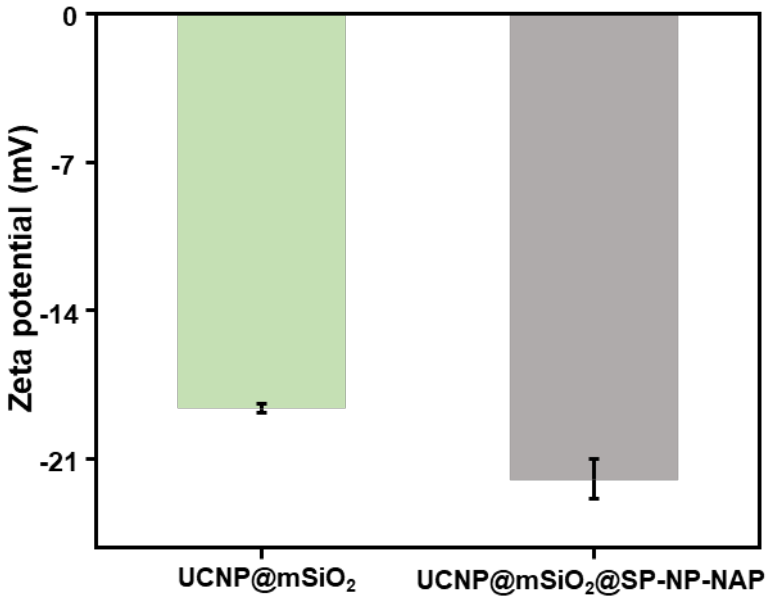

Fig. S20. Zeta potentials of UCNP@mSiO$_2$ and UCNP@mSiO$_2$@SP-NP-NAP.

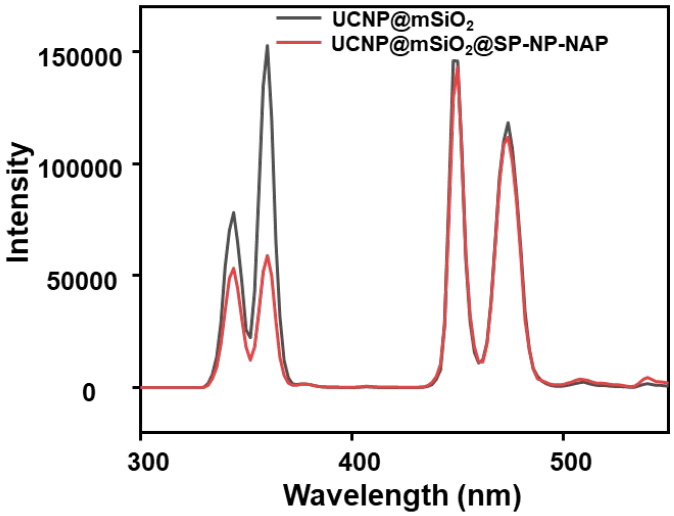

Fig. S21. Luminescence of UCNP@mSiO$_2$@SP-NP-NAP and UCNP@mSiO$_2$ under 980 nm laser excitation.

8. Optical properties of UCNP@mSiO$_2$@SP-NP-NAP toward SO$_2$ and H$_2$S$_2$.

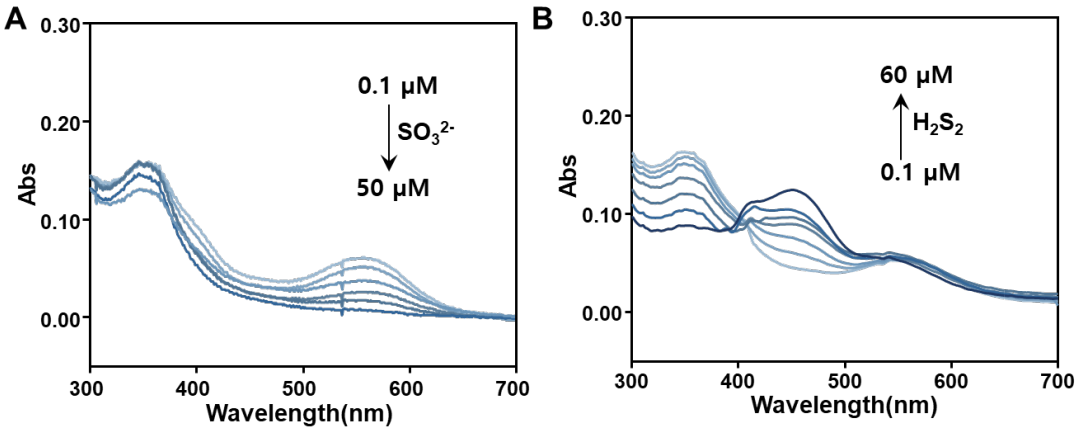

Fig. S22. The absorption spectra of UCNP@mSiO$_2$@SP-NP-NAP with different levels of (A) Na$_2$SO$_3$ (0.1-50 μM) and (B) H$_2$S$_2$ (0.1-60 μM) in PBS (10 mM, pH 7.4) under NIR/Vis light illumination, respectively.

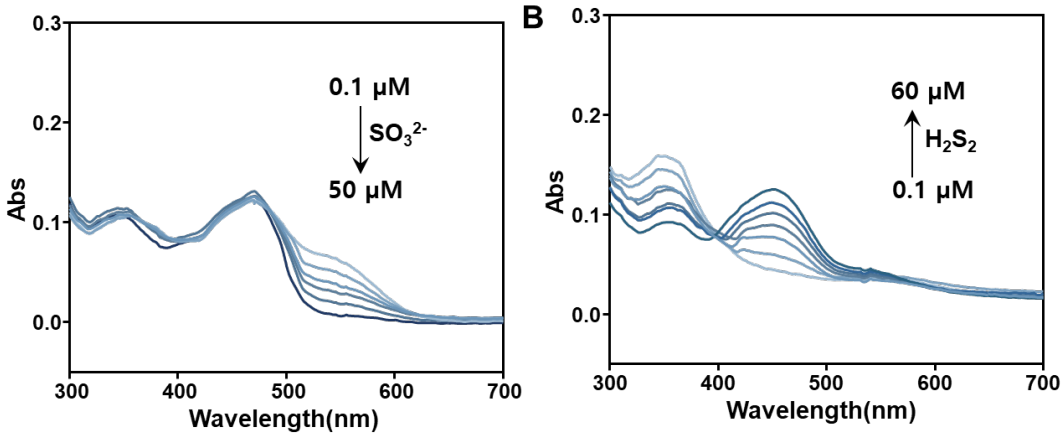

Fig. S23. The absorption spectra of UCNP@mSiO$_2$@SP-NP-NAP with different concentrations of (A) Na_2SO_3 (0.1-50 μM) in the presence of H_2S_2 (60 μM) and (B) H_2S_2 (0.1-60 μM) in the presence of Na_2SO_3 (50 μM).

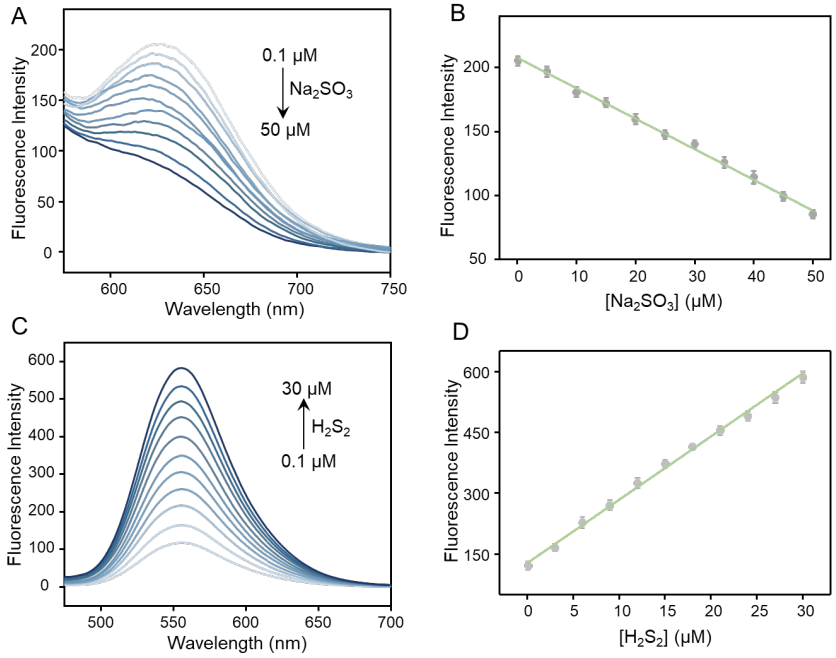

Fig. S24. The (A) fluorescence spectra and (B) the linear relationship of NIR light-activated nanoprobes for detection of Na_2SO_3 (0.1, 5, 10, 15, 20, 25, 30, 35, 40, 45, 50 μM) (λ_{ex}=540 nm) in the presence of H_2S_2 (0.1, 3, 6, 9, 12, 15, 18, 21, 24, 27, 30 μM). The (C) fluorescence spectra and (D) the linear relationship of NIR/Vis light-activated nanoprobes (B) H_2S_2 (0.1, 3, 6, 9, 12, 15, 18, 21, 24, 27, 30 μM) (λ_{ex}=460 nm) in the presence of Na_2SO_3 (0.1, 5, 10, 15, 20, 25, 30, 35, 40, 45, 50 μM). All the experiments were repeated three times and the data were shown as mean (± S.D.).

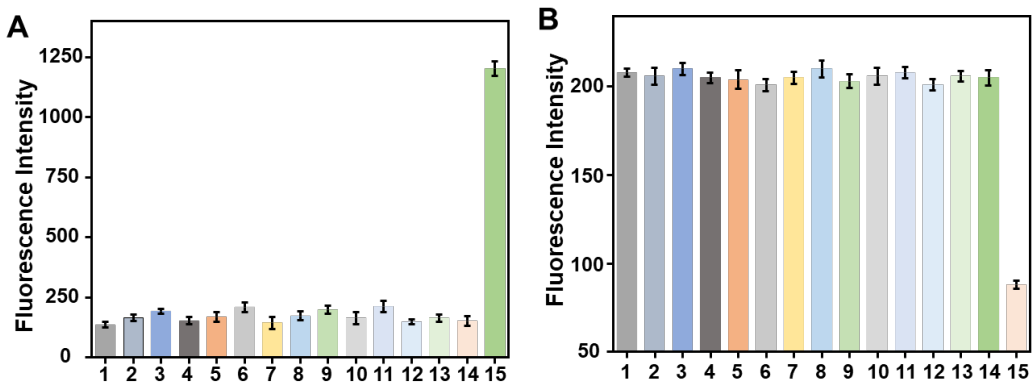

Fig. S25. Fluorescence intensity of UCNP@mSiO$_2$@SP-NP-NAP toward (A) various substances (1. Blank, 2. Cys (100 μM), 3. Hcy (100 μM), 4. GSH (100 μM), 5. $NaNO_2$ (100 μM), 6. $NaNO_3$ (100 μM), 7. NAC (100 μM), 8. Br^- (100 μM), 9. I^- (100 μM), 10. Cl^- (100 μM), 11. S^{2-} (100 μM), 12. CO_3^{2-} (100 μM), 13. ClO^- (100 μM), 14. H_2O_2 (100 μM), 15. S_2^{2-} (60 μM)) at 550 nm, and (B) various substances (1. Blank, 2. Cys (100 μM), 3. Hcy (100 μM), 4. GSH (100 μM) , 5. NAC (100 μM), 6. SO_4^{2-} (100 μM), 7. SCN^- (100 μM), 8. F^- (100 μM), 9. Cl^- (100 μM), 10. Br^- (100 μM), 11. I^- (100 μM), 12. CO_3^{2-} (100 μM), 13. Na^+ (100 μM), 14. K^+ (100 μM), 15. Na_2SO_3 (50 μM)) at 640 nm. All the experiments were repeated three times and the data were shown as mean (± S.D.).

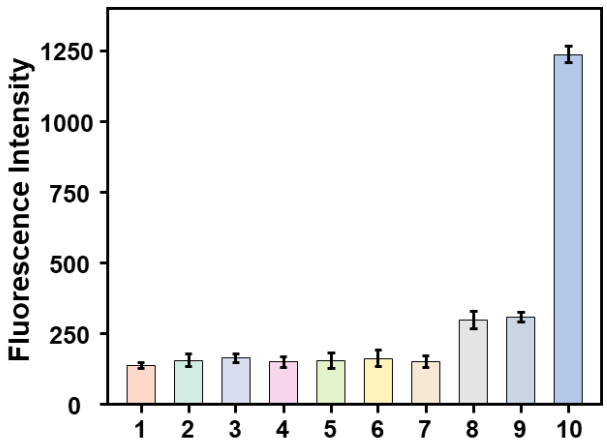

Fig. S26. Fluorescence intensity of UCNP@mSiO$_2$@SP-NP-NAP toward persulfides, hydropersulfides and protein persulfides at 550 nm. 1. blank, 2. $Na_2S_2O_4$, 3. $Na_2S_2O_5$, 4. CysSSCys, 5. CH_3SSSCH_3, 6. papain, 7. GAPDH, 8. GSSH, 9. CysSSH, 10. Na_2S_2. The concentrations of all substances were 60 μM. All the experiments were repeated three times and the data were shown as mean (± S.D.).

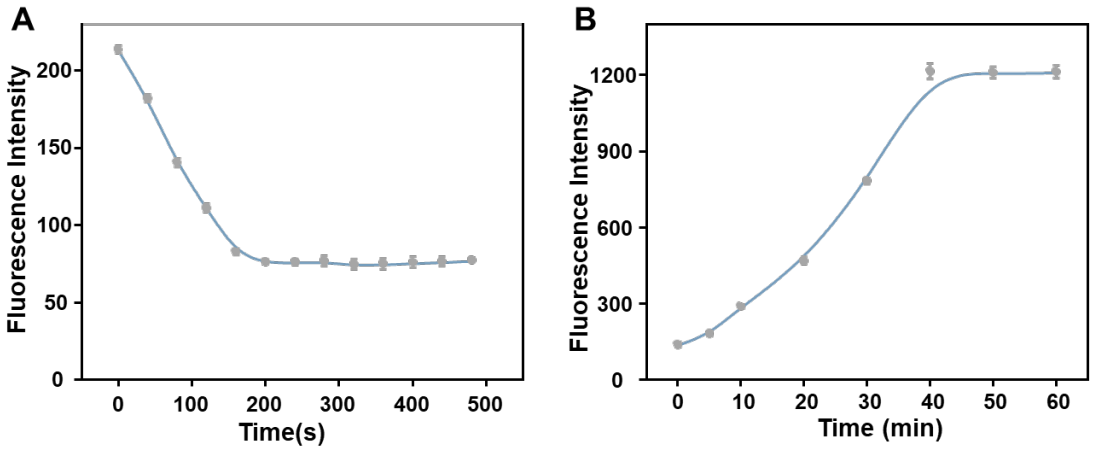

Fig. S27. Time-dependent fluorescence intensity of UCNP@mSiO$_2$@SP-NP-NAP toward (A) Na_2SO_3 (50 μM) (λ_{ex}=540 nm) after activated by NIR irradiation (980 nm) and (B) H_2S_2 (60 μM) (λ_{ex}=460 nm) after activated by Vis light (550 nm). All the experiments were repeated three times and the data were shown as mean (± S.D.).

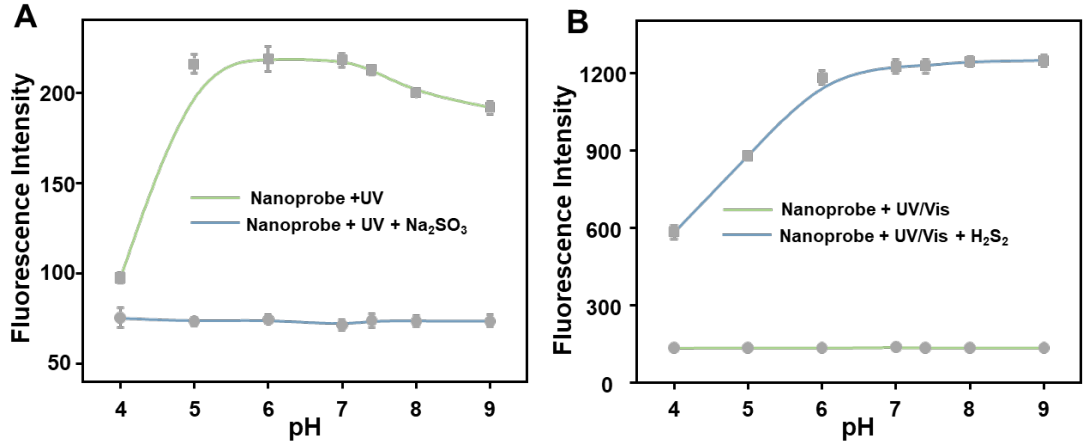

Fig. S28. pH-dependent fluorescence intensity of UCNP@mSiO$_2$@SP-NP-NAP toward (A) Na_2SO_3 (50 μM) (λ_{ex}=540 nm) after NIR light (980 nm) activation and (B) H_2S_2 (60 μM) (λ_{ex}=460 nm) after NIR (980 nm) and Vis (550 nm) light irradiation. All the experiments were repeated three times and the data were shown as mean (± S.D.).

9. Cytotoxicity and imaging studies of UCNP@mSiO$_2$@SP-NP-NAP.

Cytotoxicity of UCNP@mSiO$_2$@SP-NP-NAP.

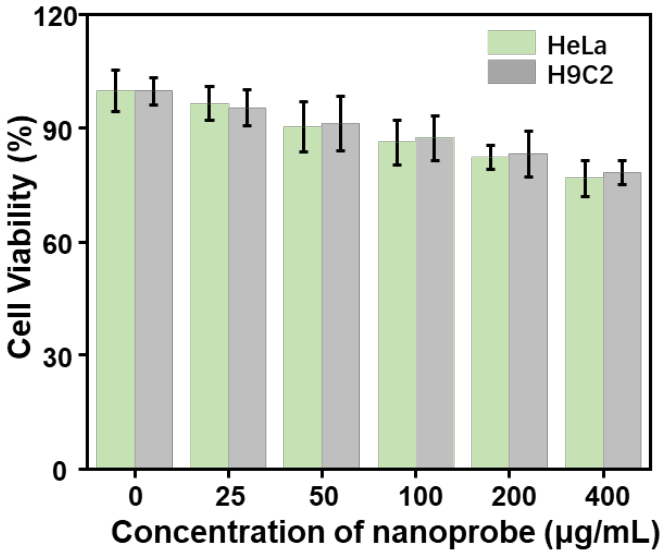

Fig. S29. Cell viability of H9C2 and HeLa cells after incubation with different concentrations of nanoprobe (0-400 μg/mL).

Imaging of SO_2 and H_2S_2 via UCNP@mSiO$_2$@SP-NP-NAP in living cells.

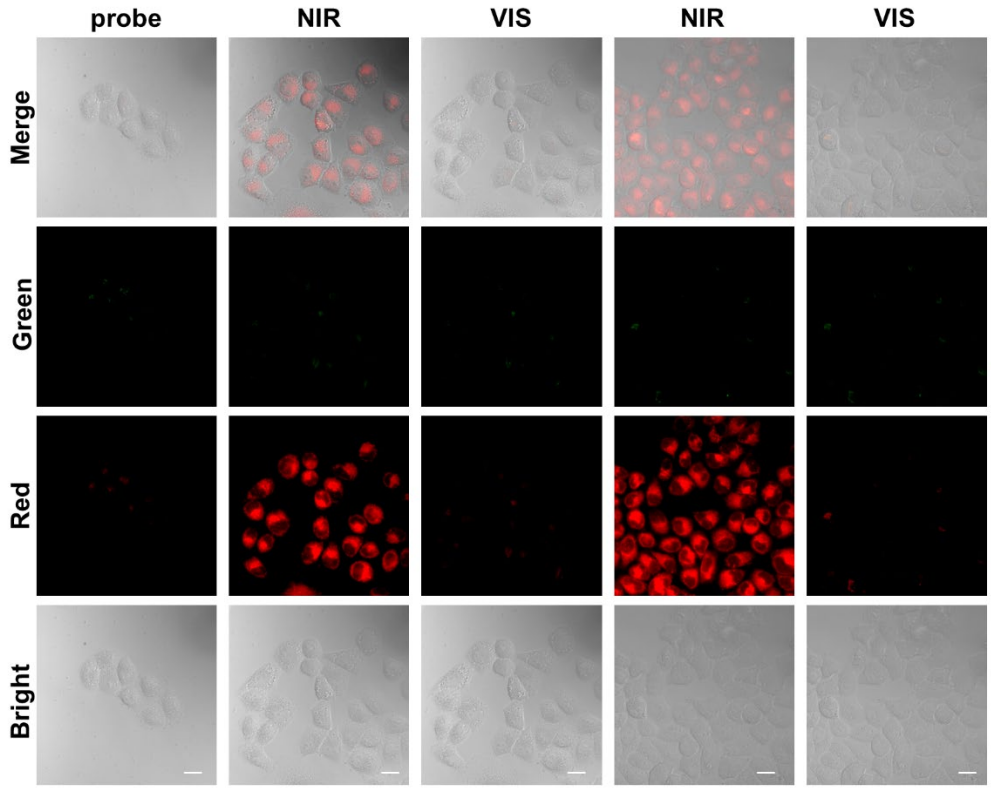

Fig. S30. Confocal laser scanning microscopy image HeLa cells incubated with UCNP@mSiO$_2$@SP-NP-NAP under alternative NIR/Vis light irradiation. NIR light irradiation for 30 min; Vis light irradiation for 10 min. Vis light irradiation was performed after NIR light irradiation. Red fluorescent channel: λ_{em} = 610 - 670 nm (λ_{ex}

= 561 nm); green fluorescent channel: λ_{em} = 520 - 580 nm (λ_{ex} = 488 nm), Scale bar: 20 μm.

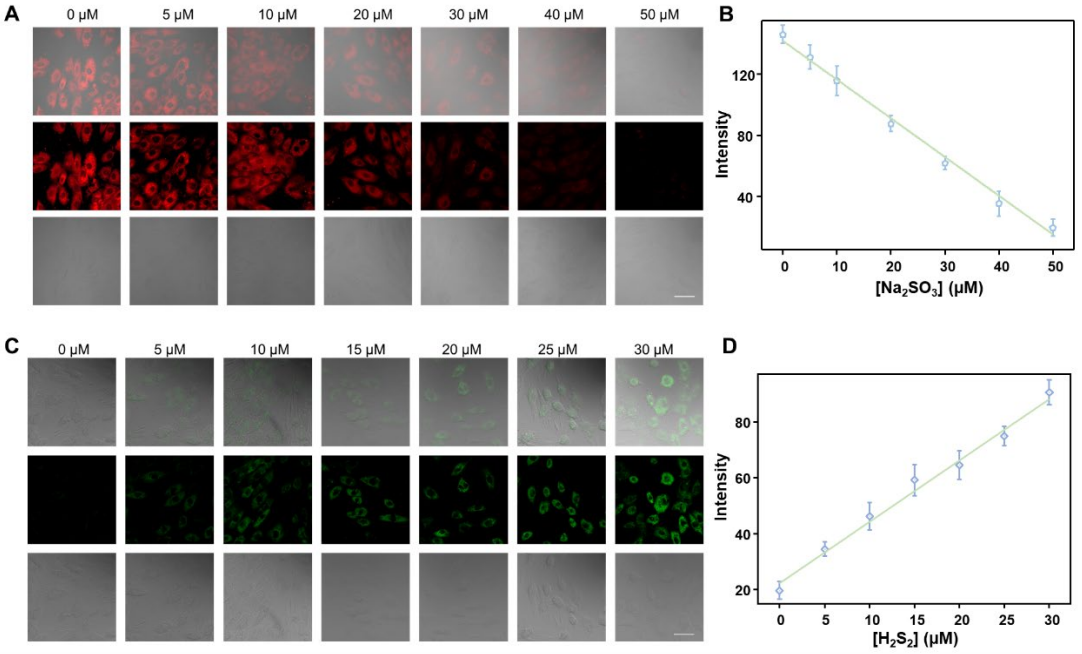

Fig. S31. Fluorescence images of H9C2 cells treated with different concentrations of Na_2SO_3 and H_2S_2. (A) Fluorescence images and (B) the linear relationship of NIR light-activated nanoprobe for different concentrations of Na_2SO_3 in the presence of H_2S_2 (50 μM) recorded via red channel. (C) Fluorescence images and (D) the linear relationship of NIR/Vis light-activated nanoprobes for different concentrations of H_2S_2 in the presence of Na_2SO_3 (50 μM) recorded through green channel. Data are shown as the mean ± S.D. (n = 3).

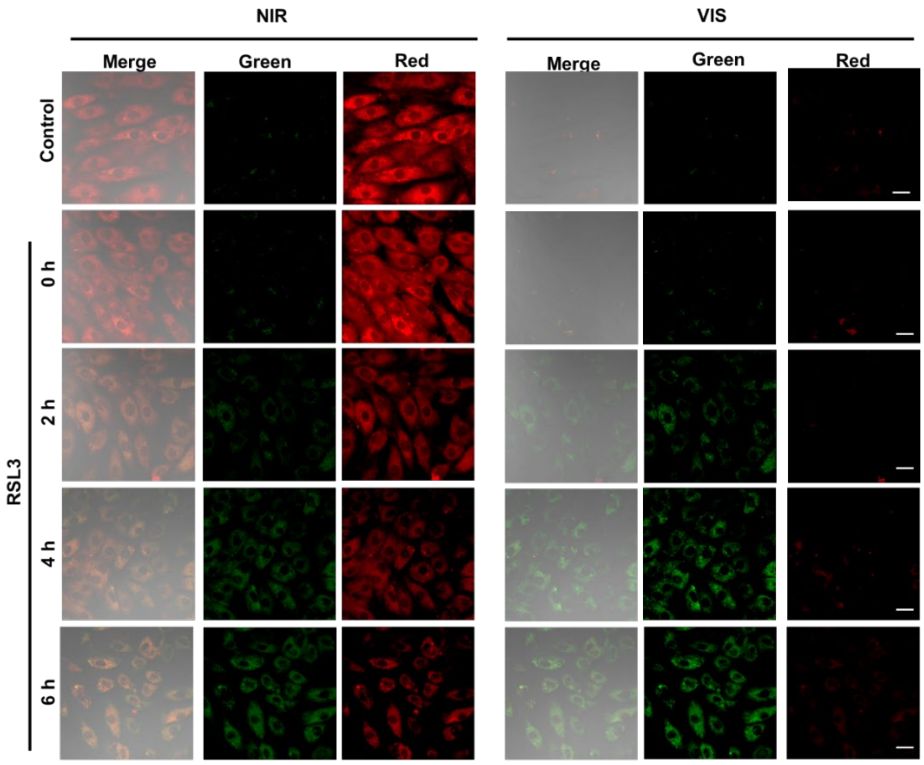

Fig. S32. The changes of SO_2 and H_2S_n levels in RSL3-treated cells at different time points. NIR light irradiation: 30 min; Vis light irradiation: 10 min. Vis irradiation is performed after NIR irradiation. Red fluorescent channel: λ_{em} = 610 - 670 nm (λ_{ex} = 561 nm); green fluorescent channel: λ_{em} = 520 - 580 nm (λ_{ex} = 488 nm), Scale bar: 20 μm.

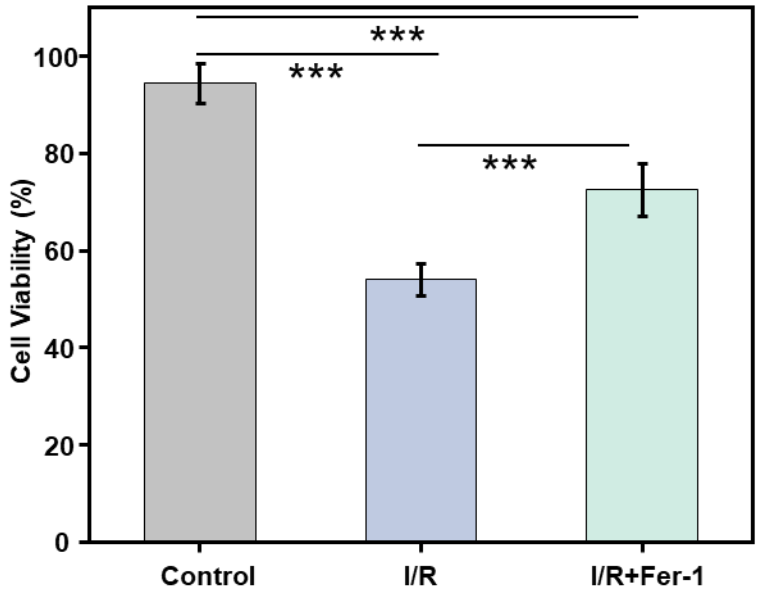

Fig. S33. Cell viability after treating H9C2 cells under different conditions. Control

group: cells were not treated; I/R group: cells were induced with I/R; I/R + Fer-1 group: cells were pre-treated with Fer-1 for 2 h prior to induction of I/R. Error bars represent mean ± S.D (n=3). from four independent replicates. Statistical significance was calculated using one way ANOVA by Tukey's multiple comparisons test. *$p < 0.05$, **$p < 0.01$, and ***$p < 0.001$.

10. References

1. T. Ida, T. Sawa, H. Ihara, Y. Tsuchiya, Y. Watanabe, Y. Kumagai, M. Suematsu, H. Motohashi, S. Fujii, T. Matsunaga, M. Yamamoto, K. Ono, N. O. Devarie-Baez, M. Xian, J. M. Fukuto, T. Akaike, Reactive cysteine persulfides and S-polythiolation regulate oxidative stress and redox signaling. *Proc. Natl. Acad. Sci. U. S. A.,* 2014, **111**, 7606–7611.

2. X. Han, F. Yu, X. Song, L. Chen, Quantification of cysteine hydropersulfide with a ratiometric near-infrared fluorescent probe based on selenium-sulfur exchange reaction. *Chem. Sci.,* 2016, **7**, 5098–5107.

3. J. Zhang, Y. Xie, J. Ma, K. Liu, Y. Ding, Y. Li, X. Jiao, X. Xie, X. Wang, B. Tang, Real-time visualization of the fluctuations in HOBr with AIE fluorescent probes during myocardial ischemia-reperfusion injury, *Chem. Commun.,* 2023, **59**, 1018–1021.

4. H. Chen, H. Zhou, J. Yang, H. Wan, Y. He, Guhong injection mitigates myocardial ischemia/reperfusion injury by activating GST P to inhibit ASK1-JNK/p38 pathway. *Phytomedicine*, 2023, **109**, 154603.

5. X. Jiang, Y. Yu, J. Chen, M. Zhao, H. Chen, X. Song, A. J. Matzuk, Shaina L. Carroll, X. Tan, A. Sizovs, N. Cheng, M. C. Wang, J. Wang, Quantitative imaging of glutathione in live cells using a reversible reaction-based ratiometric fluorescent probe. *ACS Chem. Biol.,* 2015, **10**, 864–874.

6. Z. Liu, X. Zhou, Y. Miao, Y. Hu, N. Kwon, X. Wu, J. Yoon, A Reversible Fluorescent Probe for Real-Time Quantitative Monitoring of Cellular Glutathione. *Angew. Chem. Int. Ed.,* 2017, **56**, 5812–5816.

7. S. Hou, Y. Wang, Y. Zhang, W. Wang, X. Zhou, A reversible turn-on fluorescent probe for quantitative imaging and dynamic monitoring of cellular glutathione. *Anal. Chim. Acta,* 2022, **1214**, 339957.

8. L. Shi, C. Yan, Z. Guo, W. Chi, J. Wei, W. Liu, X. Liu, He Tian, W. H. Zhu, De novo strategy with engineering anti-Kasha/Kasha fluorophores enables reliable ratiometric quantification of biomolecules. *Nat. Commun.,* 2020, **11**, 793.